ADVANCED FUNCTIONAL MATERIALS
www.afm-journal.de

Peptide Antigen-Surfaced TLR9-Adjuvanting Nanovaccines as a Versatile Therapeutic Modality to Eradicate Acute Myeloid Leukemia

Yinping Sun, Guanhong Cui, Yan Shi, Bin Xu, Liping Qu, Fenghua Meng, and Zhiyuan Zhong**

Peptide antigen vaccines constitute a promising clinical strategy for treating cancer patients. However, their anticancer immune response remains modest because of the suboptimal presentation of peptide antigens and/or insufficient activation of antigen-presenting cells (APCs). The development of therapeutic vaccines for acute myeloid leukemia (AML) poses an even greater challenge because AML cells disseminate throughout the body. In this study, the peptide antigen-surfaced TLR9-adjuvanting nanovaccines (PASTA-NV), which display multiple Wilm's tumor 1 (WT1) peptides on their surface and encapsulate CpG ODN adjuvants within their watery interior to simultaneously increase antigen presentation and APC activation/proliferation, are reported. Interestingly, systemic administration of PASTA-NV induces strong cellular and humoral anticancer immune responses in orthotopic murine AML MLL-AF9 models. When combined with an anti-CTLA4 antibody, PASTA-NV achieves complete regression of AML in mouse models and establishes durable anti-AML immunity, effectively resisting rechallenge with leukemic cells. PASTA-NV provides a new and general avenue to induce robust and specific anticancer immunity, which has the potential to revive peptide antigen-based nanovaccines for tumor therapy.

1. Introduction

Cancer immunotherapy, including immune checkpoint blockade (ICB) and chimeric antigen-T (CAR-T) cell therapy, has heralded a new era in clinical oncology, demonstrating success against various malignancies.[1] Central to this achievement is the development of cancer vaccines that leverage tumor-associated antigens (TAAs) and tumor-specific antigens (TSAs) to prime de novo tumor-reactive T cells and activate the immune system, thereby targeting tumor cells that evade immune surveillance through antigen-specific responses. These vaccines have great potential because they target intracellular antigens, representing nearly 88% of the total protein spectrum,[2] yet face critical obstacles, such as only transient and local immune responses.[3] To circumvent these limitations, recent advancements have embraced nanotechnologies to engineer sophisticated vaccines that offer several benefits over traditional formulations, including enhanced structural and physicochemical attributes (tunable structure, size, surface, etc.), improved antigen stability (protection from nanocarriers), and targeted delivery to immune cells for recognition,[4] enabling both subcutaneous (s.c.), intravenous (i.v.), and intradermal (i.d.) administrations.

Peptide subunit vaccines harnessing tailored peptide antigens corresponding to an individual's tumor molecular profile have gained great interest for tumor therapy.[5] Peptide vaccines have the advantages of precision design, ease of manufacturing, and good safety features with noninfectious and nonreplicating natures. The nanocarriers could help to deliver and present specific epitopes resembling pattern antigens (e.g., ovalbumin) or neoantigens in cancer cells to APCs.[6] A number of peptide nanovaccines, such as ELI-002, GV1001, CDX-110, SurVaxM and ISA101, have ventured into clinical trials,[7] showcasing varying degrees of success across a spectrum of infectious diseases and cancers. Among the plethora of TAAs explored, the oncogenic protein Wilms' tumor 1 (WT1) has emerged as a prime target because of its ubiquitous expression in malignancies[8] and potential as a universal cancer vaccine target.[9] Notably, WT1 peptide-based therapeutic interventions, including subcutaneous OCV-501, have led to temporary improvements in overall survival in elderly AML patients within 4 years of follow-up.[10] AML characterized by pervasive cell dissemination and innate refractoriness poses a formidable challenge in the development of therapeutic vaccines. Notably, peptide nanovaccines typically show moderate immunogenicity and narrow-ranging immune reactions due

Y. Sun, G. Cui, Y. Shi, B. Xu, L. Qu, F. Meng, Z. Zhong
Biomedical Polymers Laboratory
College of Chemistry
Chemical Engineering and Materials Science
State Key Laboratory of Radiation Medicine and Protection
Soochow University
Suzhou 215123, P. R. China
E-mail: fhmeng@suda.edu.cn; zyzhong@suda.edu.cn
Z. Zhong
College of Pharmaceutical Sciences
Soochow University
Suzhou 215123, P. R. China

The ORCID identification number(s) for the author(s) of this article can be found under https://doi.org/10.1002/adfm.202416147

DOI: 10.1002/adfm.202416147

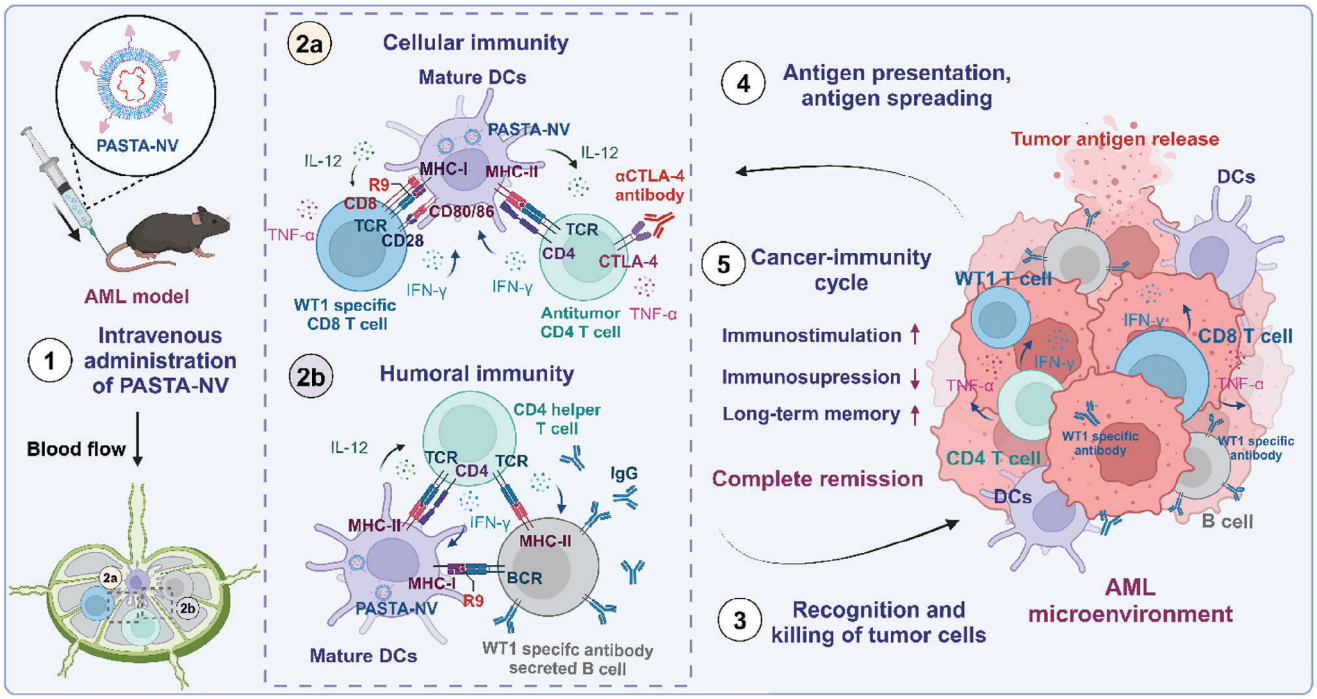

Scheme 1. Illustration of the effects of WT1 peptide antigen-surfaced TLR9-adjuvanting nanovaccine (PASTA-NV) in AML mouse models. WT1 antigenic epitopes were presented on polymersome surface at high density. The systemic administration of PASTA-NV provokes potent and durable cellular and humoral responses and effective antigen spreading, resulting in the eradication of AML and resistance to re-exposure when PASTA-NV is combined with ICB via an anti-CTLA-4 antibody.

to inefficient epitope presentation and suboptimal stimulation of APCs,[11] which collectively impair the induction of antigen-specific T-cell and antibody responses.[12]

Here, we report that peptide antigen-surfaced TLR9-adjuvanting nanovaccines (PASTA-NV), which display multiple WT1 peptides on their surface and encapsulate CpG ODN adjuvants within their watery interior, simultaneously increase antigen presentation and APC activation/proliferation. CpG ODN is a Toll-like receptor 9 (TLR9) agonist that potently induces downstream proinflammatory pathways for immune activation.[13] Notably, systemic administration of PASTA-NV induced strong cellular and humoral anticancer immune responses in orthotopic murine AML MLL-AF9 models, which, when combined with an anti-CTLA4 antibody, led to complete regression of AML and potent and durable anti-AML immunity (**Scheme 1**). PASTA-NV has the ability to induce antigen spreading and provides a new and general avenue for increasing the robust and specific anticancer immune response, which has the potential to revive peptide antigen-based nanovaccines for tumor therapy.

2. Results and Discussion

2.1. Fabrication and Characterization of PASTA-NV

WT1 peptide antigen-surfaced TLR9-adjuvanting nanovaccines (PASTA-NV) were generated via the co-self-assembly of poly(ethylene glycol)-*b*-poly(trimethylene carbonate-*co*-dithiolane trimethylene carbonate)-*b*-spermine (PEG-P(TMC-DTC)-spe)[14] and S17 peptide-functionalized PEG-P(TMC-DTC) in the presence of CpG (nanovaccine structure shown in **Figure 1A**). The S17 peptide ($WT1_{121-137}$, SSGQARMFPNAPYLPSC) consists of a universally recognized and minimally defined antigenic epitope, R9 ($WT1_{126-134}$, RMFPNAPYL),[8b] and some extended amino acids around R9 from the sequence of the WT1 protein. This long peptide may be loaded on MHC II molecules and promote robust cross-presentation and stimulation of the $CD4^+$ T-cell response. Celis et al. reported that $WT_{122-138}$, with some extra amino acids beyond R9, acted as a $CD4^+$ T-cell epitope stimulating peptide-specific responses, such as cytokine secretion, and clinical data showed that the extended sequence facilitated the presentation of MHC II molecules, which then induced a $CD4^+$ T-cell response.[15] S17-PEG-P(TMC-DTC) was obtained by treating maleimide-functionalized PEG-P(TMC-DTC)[16] with a cysteine-terminated S17 peptide. ^{1}H-NMR spectra and MicroBCA assays indicated close to 100% peptide functionalization (Figures S1 and S2, Supporting Information). Notably, PASTA-NV with an S17 surface density of 30 mol.% displayed a size of ≈60 nm, narrow distribution (PDI: ≈0.1), and neutral zeta potentials (Figure 1B; Table S1, Supporting Information). The nanovaccines without S17 peptide (TA-NV) were prepared with similar properties from the self-assembly of PEG-P(TMC-DTC)-Spermine in CpG-containing solution. The mixture of TA-NV with free S17 peptide, denoted S17/TA-NV (Table S2, Supporting Information), was used as a control for later studies. Notably, surface-displayed S17 peptides on polymersomes may provide advantages over free peptides and those encapsulated inside polymersomes, including better recognition by proteasomes,

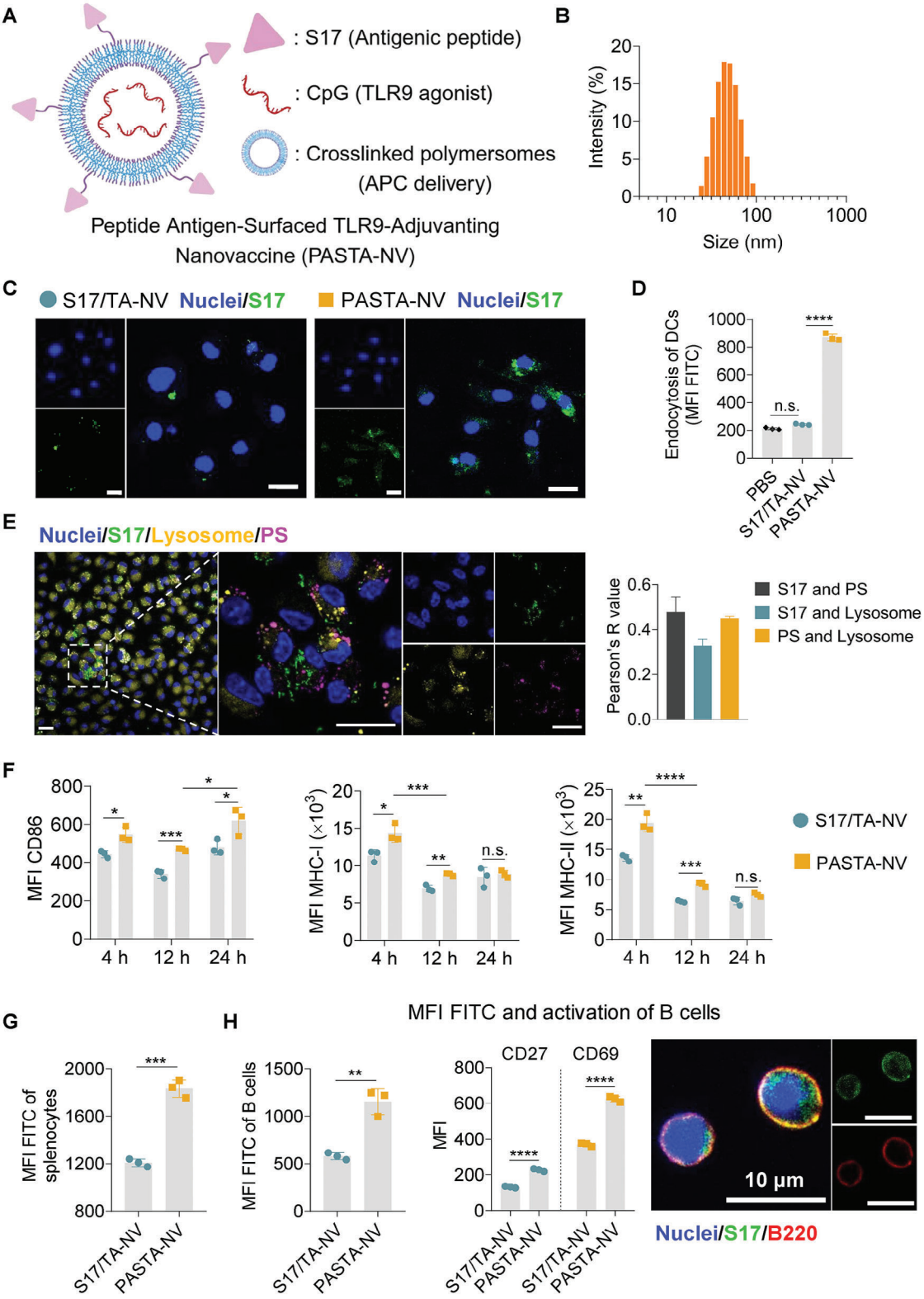

Figure 1. In vitro characteristics of PASTA-NV. A) Illustration of the structure and B) size distribution of PASTA-NV determined by DLS. Endocytosis of PASTA-NV and S17/TA-NV in BMDCs determined by C) CLSM and D) FC at 4 h incubation. E) Lysosome escape study using CLSM at 4 h incubation. F) The expression of CD86, MHC-I and MHC-II molecules of BMDCs by PASTA-NV at the indicated time points. G) MFI of FITC of PASTA-NV of splenocytes. H) MFI of FITC and activation of splenic B cells treated with PASTA-NV. For C–H, FITC-labeled S17 was used to construct PASTA-NV. The scale bars in C and E represent 20 μm, and those in H represent 10 μm. $n = 3$ for D–H. * $p < 0.05$, ** $p < 0.01$, *** $p < 0.001$, and **** $p < 0.0001$.

longer retention in the cytosol of APCs, and the potential to elicit a B-cell response.[17]

2.2. Immune Activation Potential of PASTA-NV In Vitro

We used a FITC-labeled S17 peptide as a model to assess the cellular uptake, activation and antigen presentation of PASTA-NV in BMDCs (bone marrow-derived dendritic cells from C57BL/6 mice). Confocal laser scanning microscopy (CLSM) images after 4 h incubation revealed clear cytosolic delivery of S17 to BMDCs by PASTA-NV compared with the negligible fluorescence observed in the S17/TA-NV group (Figure 1C). Flow cytometry confirmed a 3.59-fold increase in the uptake of PASTA-NV by BMDCs relative to that of S17/TA-NV (Figure 1D). The results of intracellular trafficking studies using fluorescently labeled polymersome (PS), S17 and endolysosomes revealed that after 4 h incubation, both the polymersomes and S17 exhibited low colocalization with endolysosomes, indicating efficient lysosomal escape of PASTA-NV and the release of S17 into the cytosol (Figure 1E). During this process, it was expected that some conjugated S17 could be cleaved from the polymersomes by enzymes in endolysosomes or in the cytosol. In endolysosomes, cleaved S17 peptides were processed to bind MHC II molecules to stimulate the $CD4^+$ T-cell response. In the cytosol, escaped conjugated S17 and released S17 were recognized by proteasomes and loaded by MHC I molecules to present antigens, thus stimulating the $CD8^+$ T-cell response. Notably, PASTA-NV triggered significantly elevated expression of CD86, MHC-I and MHC-II molecules (the sources of the antibodies used are listed in Table S3, Supporting Information) compared with the S17/TA-NV control, indicating better DC stimulation and overall antigen presentation ability (Figure 1F). PASTA-NV increased DC maturation at 4, 12, and 24 h, whereas MHC-I and MHC-II expression were enhanced at only 4 and 12 h. Furthermore, PASTA-NV significantly increased the mean fluorescence intensity (MFI) of FITC and activation signals (CD27 and CD69) in total splenocytes and B cells (Figure 1G,H), with S17 distributed within and on the B cells, as portrayed in CLSM images (Figure 1H). These results demonstrate that PASTA-NV significantly increases the uptake, stimulation and overall antigen presentation ability of APCs, including DCs and B cells.

2.3. In Vivo Enhancement of Antigen Cross-Presentation and APC Activation by PASTA-NV

We established orthotopic MLL-AF9 mouse AML models (MA9 mice) as previously reported[18] and used Cy5-labeled CpG as a probe to investigate the in vivo effect of PASTA-NV on antigen uptake and activation of APCs upon single intravenous (i.v.) injection (**Figure** 2A). Figure 2B shows extensive immunofluorescence across key immune organs, such as the spleen, at 6 h post injection, indicating the dissemination of PASTA-NV to immune cells, such as DCs, macrophages and B cells. Notably, B cells and DCs were located mainly in the red pulp within the spleen (Figure 2B). This is attributed primarily to the accumulation of these immune cells, which had endocytosed PASTA-NV during circulation, and/or their migration from the white pulp for targeted interaction with PASTA-NV, which marks an important step toward targeted immunomodulation and engagement. FACS analyses revealed increased total uptake of PASTA-NV by APCs, with 2–3.5-fold increases in total Cy5-CpG^+ splenocytes, Cy5-CpG^+ DCs and Cy5-CpG^+ macrophages (Figure 2C,D). The spleen APCs exhibited superior activation and antigen presentation capabilities, as demonstrated by enhanced expression of MHC I and MHC II molecules when they were exposed to PASTA-NV (Figure 2E). Investigations on inguinal lymph nodes (LNs) also revealed significant PASTA-NV colocalization with DCs and macrophages (Figure S3, Supporting Information), which may reinforce in vivo immunogenicity and T-cell priming. Figure 2F displays elevated secretion of proinflammatory cytokines (IL-1α, IFN-γ, TNF-α, and IL-27), supporting enhanced immune activation.

We then assessed the longevity of the effects of PASTA-NV in MA9 mice following an extended immunization schedule (**Figure** 3A). The results revealed 3.9-fold amplification in plasmacytoid dendritic cell (pDC) populations and pronounced elevations in the expression of an activation marker (CD80) across the conventional dendritic cell (cDC) spectrum within the spleen as well as propagated cDCs within LNs (Figure 3B–D), which is pivotal for efficient T-cell priming. cDC subsets, type 1 (cDC1) and type 2 (cDC2) lineages, which professionalize at cross-presentation for priming of $CD8^+$ T cells and $CD4^+$ T cells, respectively,[19] demonstrated obvious propagation and activation across the spleen and inguinal LNs, culminating in highly exhaustive T-cell priming.

2.4. PASTA-NV Enhanced Anti-AML Efficacy via Amplified Cellular and Humoral Immunity

The results of the therapeutic studies revealed that i.v. injection of PASTA-NV significantly retarded AML progression in vivo (Figure 3E) and extended the median survival time (MST) of MA9 mice (MST: 55 days vs 44 and 41 days for S17/TA-NV and PBS control groups, respectively) (Figure 3F). To elucidate the underlying mechanism, the cellular and humoral immunity elicited by PASTA-NV was assessed. Figure 3G shows significant NK cell activation in peripheral blood (PB), which may lead to early restrictions on AML progression. Additionally, the systemic IL-12p70 level in PB of PASTA-NV group at 6 h after the last dosage surged (Figure 3H), which has been acknowledged critical for the upregulation of sustained IFN-γ expression by T cells. Such dynamics are crucial for instigating antigen spreading in vivo, thereby fueling a cancer-immunity cycle to achieve long-term tumor eradication.[20]

B cells have a strong effect on the overall antitumor effect.[21] Building on the high uptake by B cells (Figure 1I), PASTA-NV significantly enhanced serum antibodies against the specific epitope $WT1_{126\text{-}134}$ (Figure 3I), confirming tailored activation and humoral response induction by B cells. Specific antibodies can detect and expose MHC-I-presenting epitopes on tumor cells to the immune system. Antibodies against $WT1_{126\text{-}134}$ are positively associated with better clinical outcomes.[22] Further exploration of the spleen demonstrated surged contents of PD-1^+CXCR5^+ follicular helper T cells (Tfhs), $B220^+$ B cells, and increased CD27 expression on B cells (indicating the memory differentiation

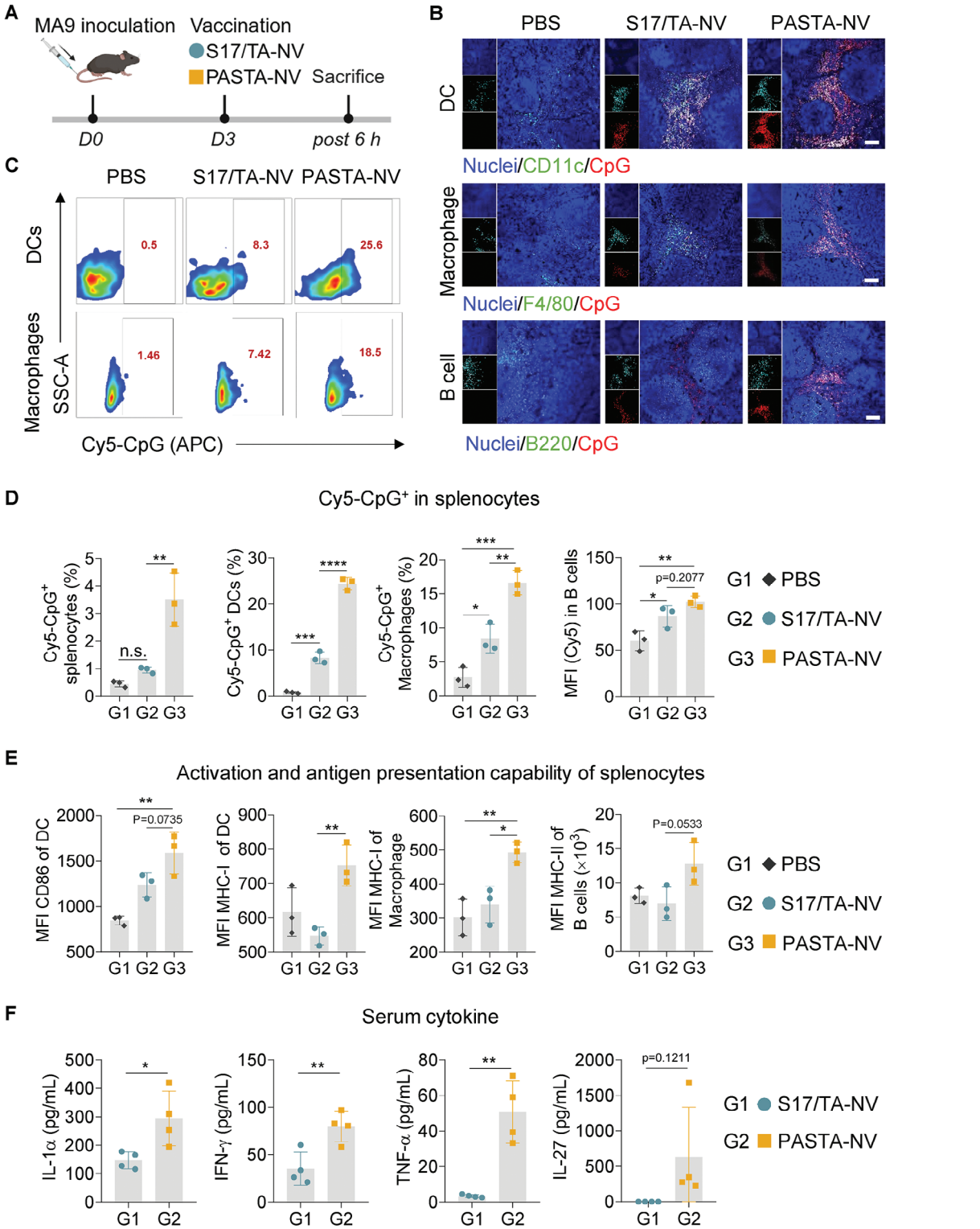

Figure 2. Biodistribution of PASTA-NV in immune cells and their activation upon a single intravenous injection in MA9 mice. A) Schematic illustration of AML inoculation, immunization and analysis. The mice were inoculated with MA9 cells on day 0, and PASTA-NV (with Cy5-labeled CpG) was i.v. injected on day 3. Spleens, LNs, bones and serum samples were measured at 6 h postinjection. B) Representative immunofluorescence (IF) images showing the colocalization of PASTA-NV within spleen DCs, macrophages and B cells (scale bar: 100 μm). C) Representative FC histograms showing the uptake of PASTA-NV by DCs, macrophages and B cells. D) The percentages of Cy5-CpG$^+$ cells in splenocytes, DCs and macrophages, and the MFI of Cy5 in B cells ($n = 3$). E) The expression of CD86, MHC-I and MHC-II molecules in various immune cells in the spleen ($n = 3$). F) Secretion of serum cytokines (IL-1α, IFN-γ, TNF-α, and IL-27) by vaccinated mice ($n = 4$). * $p < 0.05$, ** $p < 0.01$, *** $p < 0.001$, and **** $p < 0.0001$.

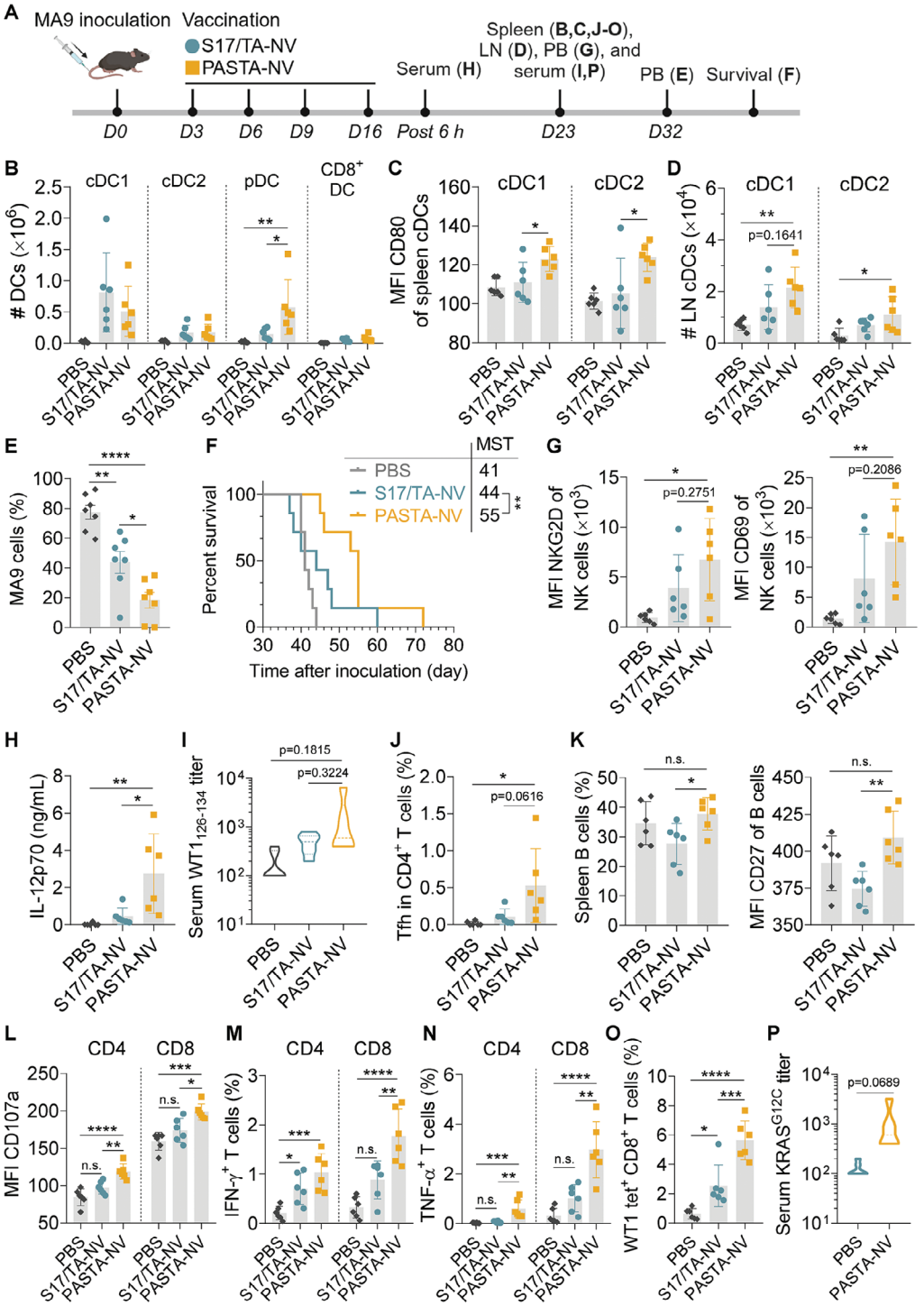

Figure 3. PASTA-NV induced potent cellular and humoral responses in MA9 mice. A) Schematic illustration of AML inoculation, immunization and analysis. PASTA-NV and S17/TA-NV were i.v. injected, and PBS was used as a control. B) Counts of spleen DC subsets ($CD103^+$cDC1, $CD11b^+$cDC2, $B220^+$pDCs, and $CD8^+$DC, gated in $CD11c^+MHC\text{-}II^+$ DCs). C) MFI of CD80 in cDC1s and cDC2s within the spleen. D) Counts of LN DC subsets ($CD103^+$cDC1s and $CD11b^+$cDC2s, gated on $CD11c^+MHC\text{-}II^+$ DCs). E) MA9 cell infiltration in the peripheral blood (PB) on day 32 (data are presented as the mean ± SEM). F) Survival curves of MA9 mice. G) Activation of NK cells and MFI of NKG2D and CD69 in PB on day 23. H) Serum levels of IL-12p70 at 6 h after the last vaccination. I) Serum specific titers of the $WT1_{126\text{-}134}$ peptide. J) Percentages of $PD\text{-}1^+CXCR5^+$ Tfhs among splenic $CD4^+$ T cells. K) Percentages of splenic $B220^+$ B cells and the MFI of $CD27^+$ B cells. L) Degranulation of T cells (MFI of CD107a in splenic $CD4^+$ T cells and $CD8^+$ T cells). Percentages of M) IFN-γ^+ and N) TNF-α^+ T cells among splenic $CD4^+$ T cells and $CD8^+$ T cells. O) Percentages of $WT1_{126\text{-}134}$-specific T cells among splenic $CD8^+$ T cells. P) Serum specific titers of the $KRAS^{G12C}$ mutant epitope. Sample number $n = 7$ for infiltration and survival studies (E,F), and $n = 6$ for analysis on day 23 (B,D, G,P). * $p < 0.05$, ** $p < 0.01$, *** $p < 0.001$ and **** $p < 0.0001$.

status) compared to S17/TA-NV group (Figure 3J,K). Tfhs are essential for B-cell affinity, maturation and differentiation into memory B cells.[23] Our findings suggest a symbiotic Tfh-B-cell interaction pivotal for the initiation and sustainability of the humoral immune response against AML.

Within the spleen of the PASTA-NV group, significant upregulation of CD107a expression (T-cell degranulation) and IFN-γ^+ and TNF-α^+ T cells across CD4$^+$ and CD8$^+$ T cells were detected (Figure 3L–N). In particular, the elevated secretion of IFN-γ by CD8$^+$ T cells and CD4$^+$ T cells (Figure 3M) indicates the upregulation of MHC-I and MHC-II molecules on tumor cells and APCs, respectively. MHC-I upregulation on tumor cells and MHC-II upregulation on APCs may yield more efficient antigen presentation and further eradication of tumor cells. The detection of a prominently elevated population of $WT1_{126\text{-}134}$ tetramer$^+$ CD8$^+$ T cells (***, Figure 3O) unequivocally demonstrated the precision and efficacy of the antigen-specific T-cell response elicited by PASTA-NV.

Furthermore, the antigen spreading effect elicited by PASTA-NV was detected, as evidenced by surged serum antibodies against a nonimmunized peptide, the KRAS G12C mutant epitope ($KRAS_{5\text{-}14}$: KLVVVGACGV) (Figure 3P).[24] A large increase in systemic IL-12p70, which is indispensable for antigen spreading, was also observed (Figure 3H).[25] The results indicate an expanded repertoire of the immune response beyond the initially targeted antigens, reigniting a durable adaptive antitumor immune response. This antigen spreading effect of PASTA-NV reveals the potential of this "off-the-shelf" nanovaccine. Collectively, these results highlight the synergistic immune activation of PASTA-NV in promoting robust and durable cellular and humoral responses against AML.

2.5. Vaccination Strategy of PASTA-NV Dictated Biodistribution and Antileukemic Potency

Vaccination regimens may have various impacts on the breadth and depth of innate and adaptive immunity.[26] We investigated the influence of vaccination strategy, i.e., all i.v. injections, all subcutaneous (s.c.) injections, and two s.c. followed by two i.v. injections (s.c. + i.v.) at the same dose on disease modulation and survival outcomes (**Figure** 4A). Interestingly, our results showed that all i.v. injections manifested the best inhibition of MA9 cell infiltration in the bone marrow, with undetectable AML cell infiltration in 5/6 of the mice on day 23 (Figure 4B), accordingly the best survival (Figure 4C).

To clarify the impact of vaccination strategies on biodistribution and engagement with diverse immune cells, PASTA-NV encapsulating Cy5-tagged CpG was administered to MA9 mice (Figure 4A). Six hours after the last injection, the spleen, LNs, and bone marrow were collected for analysis (Figure 4D). Ex vivo quantification highlighted a pronounced Cy5 signal in the spleens of all i.v. group, surpassing those in s.c.+i.v. and all s.c. groups, whereas the LNs exhibited a heightened Cy5 intensity in all s.c. group (Figure S4A, Supporting Information). Representative IF images of whole spleen sections revealed the dominant localization of PASTA-NV within the red pulp for all i.v. group, which highly colocalized with B cells and DCs (Figure 4E; Figure S4B, Supporting Information). In sharp contrast, for all s.c. group, B cells exclusively remained in the white pulp, whereas for s.c.+i.v. group, the B cell distribution and colocalization were between those of the other groups. For macrophages, very low localization was observed for all three groups, indicating that PASTA-NV was primarily chaperoned into the spleen by B cells and DCs. The spleen is a gatekeeper of systemic immunity, where DCs are responsible for capturing and presenting antigens to activate T cells, and B cells are responsible for antibody responses against blood-borne antigens.[27] Interestingly, follicle B cells migrated into the marginal zone to be exposed to the i.v. injected PASTA-NV (Figure 4E), which is distinctive from the other two groups. Detailed FACS analysis of the spleens revealed 2.5–9.7-fold greater Cy5 intensity in total splenocytes and 2.3–10.5-fold greater Cy5 intensity in DCs in the all i.v. group compared to other groups, while the differences in the mean uptake by macrophages and B cells were less (Figure 4F).

Moreover, bone marrow analyses revealed a significantly augmented Cy5 signal within B cells in the all i.v. group, accompanied by increased MHC-I and MHC-II expression (Figure S4C, Supporting Information). Interestingly, all three vaccination strategies of PASTA-NV demonstrated penetration and colocalization with DCs and macrophages within LNs (Figure S5, Supporting Information), indicating that effective passive delivery is mediated by migrating APCs through blood vessels or lymph vessels. These findings underscore the imperative role of the lymphatic system in mediating both local and systemic immune responses and thus in cancer immunotherapy outcomes.[28] Overall, PASTA-NV via all i.v. vaccination notably has enhanced deposition within immune organs, especially the spleen, and increased entry into immune cells to promote T-cell and humoral responses.

2.6. PASTA-NV All i.v. Vaccination Boosted Anti-AML Response via Activation of cDC1s and cDC2s

To explore the potency of PASTA-NV via i.v. administration in stimulating anti-AML responses (**Figure** 5A), we focused on the activation dynamics of cDC1s and cDC2s, since the central role of DC expansion in long-term antitumor immunity has been reported.[29] Intriguingly, a significant increase in total DC, cDC1 and cDC2 percentages was observed in inguinal LNs in the all i.v. group, significantly surpassing those in s.c.+i.v. and all s.c. groups (Figure 5B,C). Moreover, CD80 expression across the cDC1 and cDC2 subsets was consistently elevated, indicating augmented and resilient in vivo DC activation through all i.v. injected PASTA-NV compared with s.c.+i.v. and all s.c. groups (Figure 5D). Notably, s.c. injection of PASTA-NV induced considerably enlarged LNs, possibly due to the high influx of B cells, macrophages and T cells (Figure 5S), leading to a drastic decrease in DC proportions compared with those in PBS group. Within the spleens, all i.v. group also exhibited considerable increases in the cDC1 and cDC2 subsets (Figure 5E), alongside pronounced expansion in B cell population and CD27 expression (Figure 5F,G).

Furthermore, for all i.v. and all s.c. groups, the results of the splenocyte assays post-ex vivo S17 peptide re-exposure revealed amplified CD4$^+$ and CD8$^+$ T-cell degranulation (Figure 5H) and increased IFN-γ^+ and TNF-α^+ T-cell proportions compared to s.c.+i.v. group (Figure 5I,J). Notably, within the spleen, all

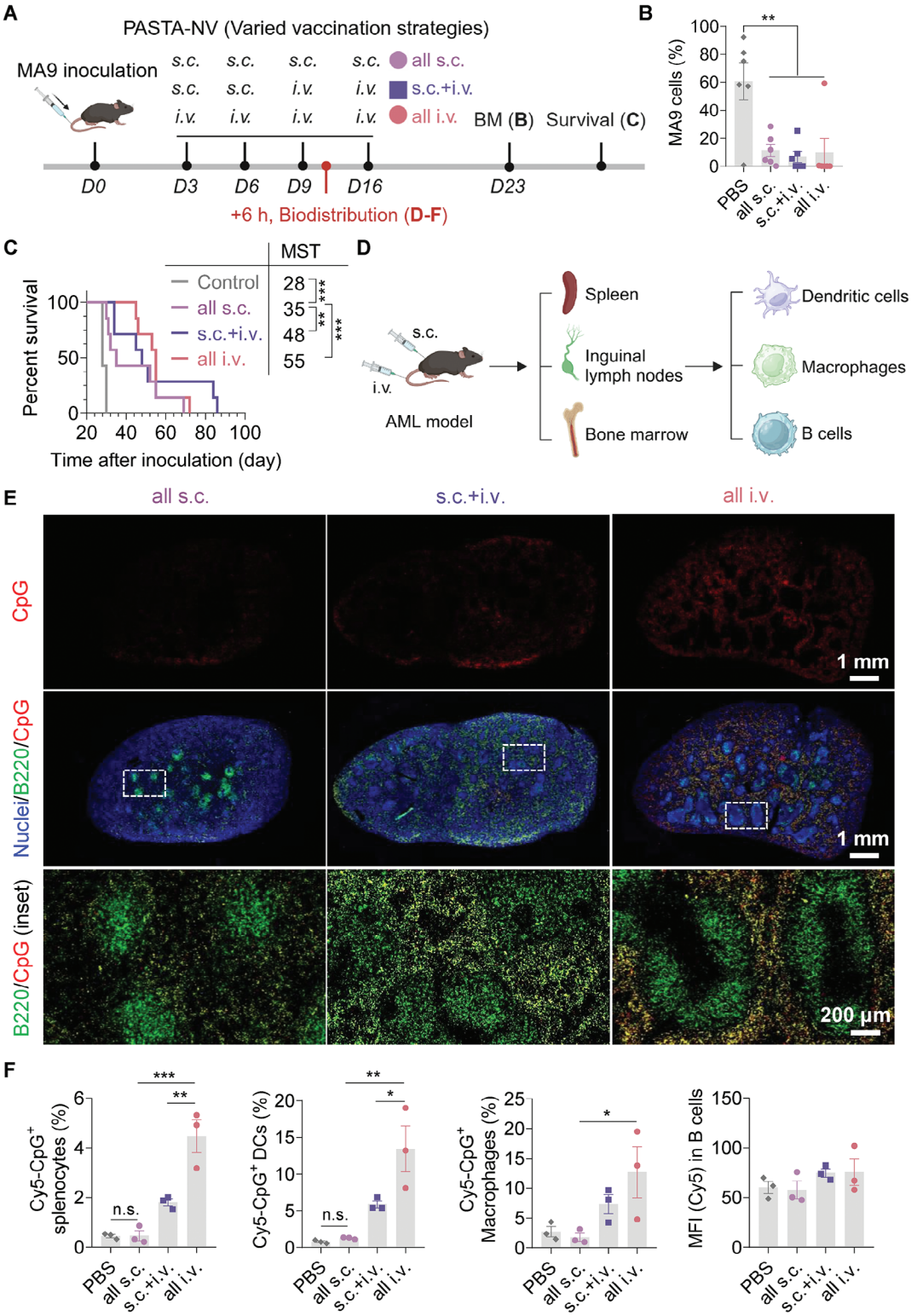

Figure 4. Vaccination strategies dictated the antitumor potency and biodistribution of PASTA-NV in MA9 mice. A) Schematic illustration of AML inoculation, vaccination strategies and analysis. B) MA9 cell infiltration in the bone marrow on day 23 ($n = 6$, data are presented as the mean ± SEM) and C) survival curves of the mice ($n = 7$). D) Illustration of the accumulation of PASTA-NV (with Cy5-labeled CpG) within major lymphoid organs and APCs. E) Representative IF images of the colocalization of PASTA-NV with splenic B cells. Scale bars: 1 mm, 1 mm, and 200 μm (top to bottom). F) Percentages of Cy5-CpG$^+$ splenocytes and Cy5-CpG$^+$ DCs and the MFI (Cy5) of PASTA-NV in macrophages and B cells within the spleens ($n = 3$). $^*p < 0.05$, $^{**}p < 0.01$, $^{***}p < 0.001$.

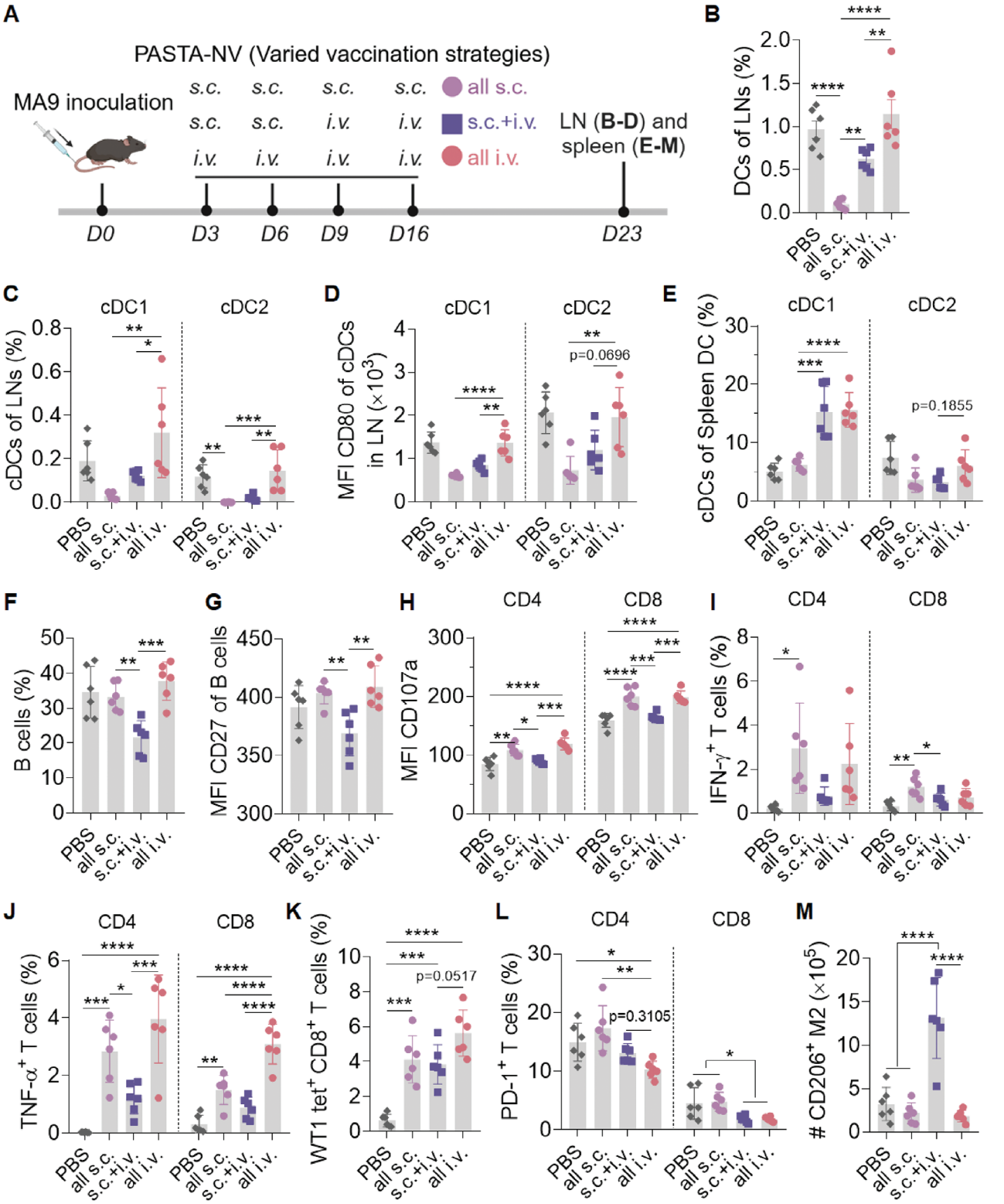

Figure 5. The vaccination strategy influenced the overall response of AML mice to PASTA-NV. A) Schematic illustration of AML inoculation, vaccination and analysis ($n = 6$). Percentages of B) total DCs, C) cDC1 and cDC2 subsets, and D) CD80 MFI of cDC1s and cDC2s within LNs. E) Percentages of cDC1s and cDC2s among splenic DCs. F) Percentages of B220$^+$ B cells and G) CD27 MFI of B cells in the spleen. H) MFI of CD107a in splenic CD4$^+$ T cells and CD8$^+$ T cells. Percentages of I) cytotoxic IFN-γ^+ T cells and J) TNF-α^+ T cells among splenic CD4$^+$ T cells and CD8$^+$ T cells after ex vivo stimulation with free S17 peptide. K) Percentages of $WT1_{126\text{-}134}$-specific CD8$^+$ T cells in the spleen. L) PD-1$^+$ CD4$^+$ and CD8$^+$ exhausted T cells in the spleen. M) Counts of CD206$^+$ M2 phenotype macrophages in the spleen. * $p < 0.05$, ** $p < 0.01$, *** $p < 0.001$, and **** $p < 0.0001$.

i.v. groups presented greater quantities of WT1-specific T cells (Figure 5K). This effect was paralleled by significantly diminished PD-1$^+$ T cells (Figure 5L) and CD206$^+$ M2 phenotype macrophages (Figure 5M), pointing to reduced T-cell exhaustion and tumor associated macrophages (TAM), respectively, both associating with poor prognosis.[30] Overall, PASTA-NV all i.v. elicits robust propagation and sustained activation of cDC1s and cDC2s while minimizing immunosuppressive PD-1$^+$ T cells and M2 macrophages, thereby triggering an optimal innate and adaptive anti-AML immune response.

2.7. Combination Therapy with PASTA-NV and α-CTLA-4 Enhanced the Immune Responses of Eradicating AML Cells

By enhancing the immunotherapeutic landscape for AML, we evaluated the synergistic potential of PASTA-NV in conjunction with ICB therapy, such as α-CTLA-4 antibody, which shows great potential for treating cancer patients.[31] The combination effect was explored by three additional i.v. injections of α-CTLA-4 (Ab, 1 mg kg^{-1}) on days 6, 9, and 16 (**Figure 6A**). Notably, the combination therapy of PASTA-NV s.c.+i.v. with Ab yielded greatly decelerated AML progression, with 3 out of 7 mice becoming tumor-free (Figure S6, Supporting Information). More impressively, the combination of PASTA-NV all i.v. with Ab (PASTA-NV+Ab) exhibited unparalleled efficacy, showcasing the eradication of AML cells by day 28 (Figure 6B) with remarkable long-term survival in 6 out of 7 mice (Figure 6C). Notably, α-CTLA-4 antibody monotherapy did not yield satisfactory outcomes, as reported in our recent work.[32]

In-depth immune analysis revealed that, compared with the PASTA-NV all i.v. group, the PASTA-NV+Ab cohort presented significantly increased CD69 expression on both CD4$^+$ T and CD8$^+$ T cells within the LNs on day 23 (Figure 6D), indicating their crucial role in the orchestration of durable and effective anti-AML responses and the establishment of local tissue-resident memory T cells.[33] Moreover, PASTA-NV+Ab therapy prominently increased DC populations, especially cDC1 and pDC subtypes (Figure 6E,F), and augmented WT1-specific CD8$^+$ T cells (Figure 6G). The significantly increased DC population was attributed to the recruitment of DCs and the differentiation from some resident monocytes stimulated by the chemokines that are secreted by activated T cells. Significant increase in total DCs is crucial for the induction of the cancer-immunity cycle. The concomitant decrease in CD4$^+$CD25$^+$FoxP3$^+$ regulatory T cells (Tregs) validated the further regulation of the immunosuppressive environment compared with PASTA-NV all i.v. group (Figure 6H). The observed enhanced mobilization of DCs may facilitate improved tumor antigen cross-presentation,[29] thus improving synergistic immune modulation. The results highlight the intricate mechanisms underlying the superior anti-AML efficacy and long-lasting immunity elicited by the combination of PASTA-NV and ICB therapy.

2.8. PASTA-NV+Ab Provided Durable Antitumor Immunity, Preventing AML Relapse

To further examine the durability of immune protection by PASTA-NV+Ab therapy, memory T cells and specific killing effects were studied in surviving mice on day 60 (Figure 6A). Analyses of PB samples revealed significant enrichment of CD44$^+$CD62L$^+$ central memory T cells (T_{CM}) and CD44$^+$CD62L$^-$ effector memory T cells (T_{EM}), which surpassed the findings in healthy naïve mice (****, Figure 6I). To mimic tumor relapse, we evaluated the capacity of memory T cells in the spleen of cured mice to be activated upon reencountering specific antigens (i.e., R9 or S17). Upon restimulation, these memory T cells rapidly proliferate and differentiate into effector T cells, including CTLs, to specifically kill MA9 tumor cells. Splenocytes isolated from a survived mouse were restimulated with long peptide S17 or shorter variant R9 (RMFPNAPYL) at two concentrations and demonstrated a dose-dependent specific anti-MA9 cell response, with S17-restimulated splenocytes displaying superior anti-AML potency at lower doses compared to R9 group. This phenomenon of an extra killing effect for S17 indicates an antigen spreading mechanism, possibly resulting from the effect of CD4$^+$ T cells,[15] as evidenced by the enhanced secretion of IFN-γ in CD4$^+$ T cells (Figure 3M). The antigen spreading occurred during PASTA-NV+Ab therapy could be partially attributed to the CTLA-4 blockade, which is known to reduce the neoantigen presentation threshold required to prime naïve T cells, thereby broadening T-cell responses.[34] Furthermore, to evaluate the role of long-term immunological defense in preventing AML relapse, the surviving mice were rechallenged with MA9 cells on day 90 (Figure 6A). During a subsequent 100-day follow-up without any therapeutic intervention, an overwhelming majority (80%) of these mice survived without signs of AML infiltration in the blood or detectable abnormalities (Figure 6K,L). Moreover, splenocytes from the surviving mice exhibited cytotoxicity against WT1-expressing tumor cell lines, such as LLC, GL261, and MC38 cells (Figure S7, Supporting Information), underscoring the potential wide application of such combination therapy in WT1-expressing tumors. Additionally, no adverse effects were observed during the experiment and the follow-up period. No damage could be discerned from H&E-stained liver slices of surviving mice at 14 months after PASTA-NV+Ab treatment (Figure S8, Supporting Information). Overall, PASTA-NV+Ab therapy has a profound effect on the propagation of DC subsets, amplifying the T-cell-mediated responses and inducing immune memory formation. This therapeutic strategy eradicates established AML and fortifies the host against future disease relapse, heralding a significant advance in cancer immunotherapy. Further improvements in the therapeutic outcomes of these nanovaccines may be achieved by improving the immunogenicity of epitopes with increased affinity for MHC molecules or TCRs, such as developing e-mimotopes.[35]

3. Conclusion

We demonstrated that WT1 peptide antigen-surfaced TLR9-adjuvanting nanovaccines (PASTA-NV) effectively treat AML-bearing mice by boosting antigen presentation and promoting APC activation/proliferation. PASTA-NV via all i.v. administration ensures optimal distribution across immune organs, including the spleen, LNs and bone marrow. This targeted delivery not only induces DC maturation and proliferation but also amplifies B cells and Tfh cells, contributing to robust priming and differentiation of T cells in MA9 AML models. Importantly,

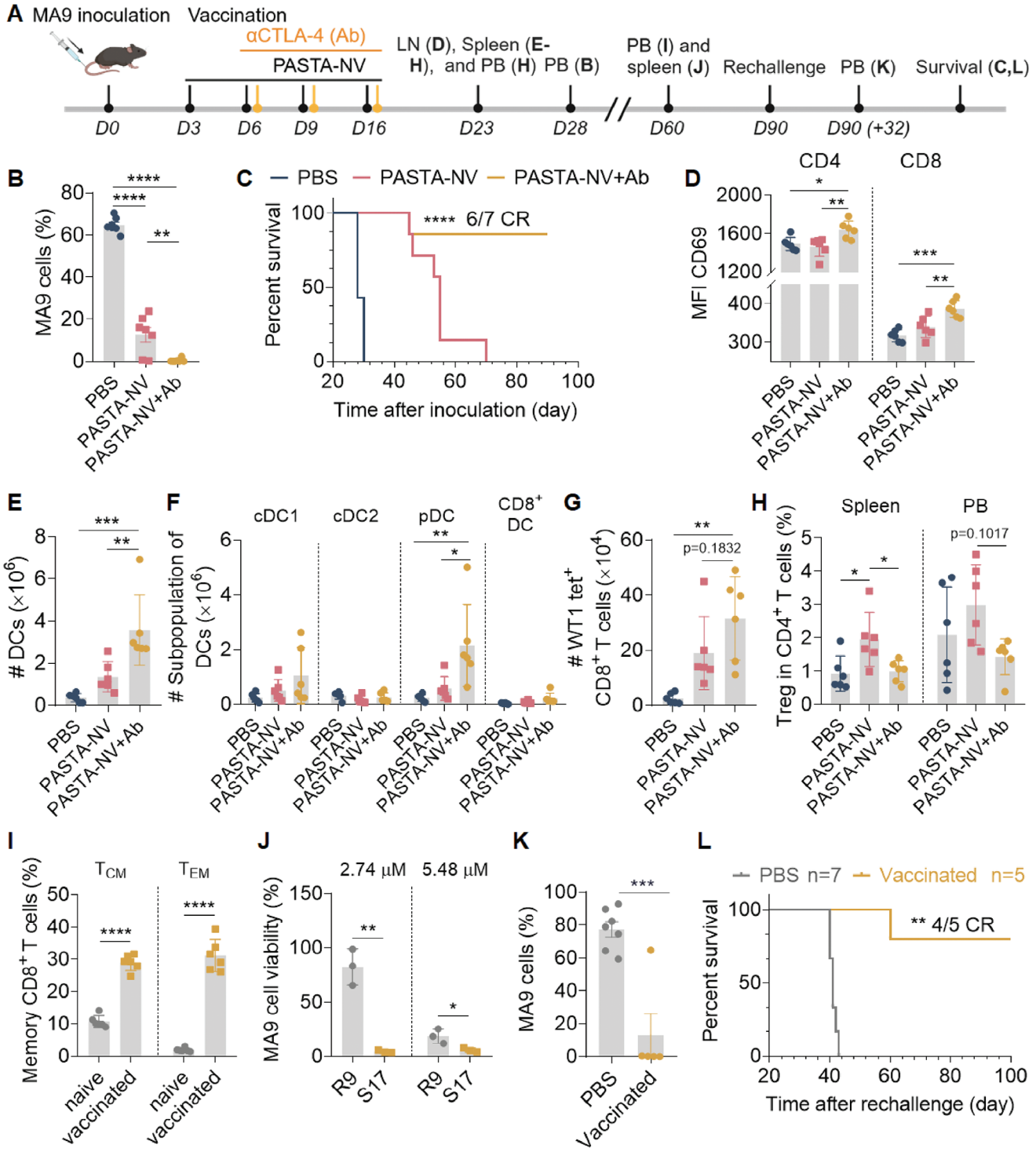

Figure 6. Combination therapy of PASTA-NV (all i.v.) with anti-CTLA-4 (PASTA-NV+Ab) boosted potent and durable anti-AML immune responses in MA9 mice. A) Schematic illustration of AML inoculation, vaccination and analysis. B) MA9 cell infiltration in the PB on day 28 and C) survival curves of the mice (n = 7). D) MFI of CD69 in $CD4^+$ and $CD8^+$ T cells in LNs. E) Counts of total DCs and F) DC subsets in the spleen. G) Counts of $WT1_{126\text{-}134}$-specific T cells in the spleen. H) Percentages of $CD25^+FoxP3^+$ Tregs among $CD4^+$ T cells in the spleen and PB. I) Percentages of central memory T cells ($CD44^+CD62L^+$ T_{CM}) and effector memory T cells ($CD44^+CD62L^-$ T_{EM}) among $CD8^+$ T cells in the PB of surviving mice on day 60. For D–I, $n = 6$. J) Specific killing of splenocytes against MA9 cells extracted from the surviving mice ($n = 3$). K) MA9 cell infiltration in PB on day 32 postchallenge and L) survival curves of rechallenged mice (rechallenged mice, $n = 5$; PBS, $n = 7$). For B and K, data are presented as the means ± SEMs. * $p < 0.05$, ** $p < 0.01$, *** $p < 0.001$, and **** $p < 0.0001$.

PASTA-NV combining with anti-CTLA-4 significantly enhances both cellular and humoral immune responses and promotes effective antigen spreading, leading to an impressive cure rate of 85% in AML mice and a potent ability to resist rechallenge by AML cells. Our study highlights the potential of peptide antigen-surfaced TLR9-adjuvanting nanovaccines based on polymersomes as a new therapeutic treatment for AML. The ability of PASTA-NV to induce effective antigen spreading presents a promising strategy for enhancing overall immune engagement in AML and potentially other WT1-expressing malignancies. Given the prevalent expression of WT1 across various cancers, such as nonsmall cell lung cancer and glioblastoma, PASTA-NV exemplifies a versatile "off-the-shelf" nanovaccine concept. This innovative peptide antigen-surfaced nanostrategy offers a flexible platform that can be adapted for treating different cancers by employing different peptide antigens and/or adjuvants.

4. Experimental Section

Synthesis of Peptide-Conjugated Polymers: Maleimide-functionalized Mal-PEG-P(TMC-DTC) (100 mg) (M_n = 7.5–15.0–2.0 kg mol^{-1}) and 10 mg of S17 peptide (M_n = 1826 g mol^{-1}, 1.34 equivalents) were dissolved in 1 mL of dimethyl formamide (DMF, AR) and stirred at room temperature. After 24 h, the mixture was dialyzed (MWCO: 7 kDa) in DMF twice to remove unbound S17 peptide and in ddH_2O trice before lyophilization to yield S17-PEG-P(TMC-DTC). The degree of peptide conjugation was determined via ^{1}H-NMR (600 MHz) and MicroBCA assays, which revealed near-quantitative conjugation.

Construction of Polymersomal Peptide Nanovaccine: PASTA-NV was prepared by mixing DMF solutions of S17-PEG-P(TMC-DTC) and PEG-P(TMC-DTC)-spe (40 mg mL^{-1}), at a mass ratio of 1:9, followed by the addition of 3.4-fold phosphate buffer (2 mM, pH 6.0) containing CpG under stirring. PASTA-NV was obtained after dialysis (MWCO: 350 kDa) in the same buffer twice and in phosphate buffer (10 mM, pH 7.4) trice. Loading content of CpG, size, and stability of PASTA-NV were determined. Nanovaccine without S17 (TA-NV) was prepared from PEG-P(TMC-DTC)-spe and CpG. The mixture of TA-NV with free S17 (denoted S17/TA-NV) was used as a control.

Uptake and Lysosome Escape of PASTA-NV within Immune Cells: FITC-labeled S17 and Cy5-labeled polymersomes were used to study the intracellular fate of PASTA-NV (S17 conc.: 0.25 μg mL^{-1}, CpG conc.: 1 μg mL^{-1}). BMDCs were seeded on 14 mm glass coverslips in 24-well plates (3×10^5 per well) overnight. PASTA-NV and S17/TA-NV were added and incubated for 4 h. The cells were gently washed, stained with LysoTracker and DAPI, fixed and then imaged via CLSM. Splenocytes were added to 24-well plates containing glass coverslips precoated with antimouse I-A/I-E antibody at 37 °C. After 2 h of incubation, the suspending cells were removed and the attached cells were treated with PASTA-NV for 4 h before fixation and blocking with 1% BSA in PBS. The cells were treated with a rat antimouse B220 antibody overnight at 4 °C, TRITC-labeled secondary antibody for 1 h at 37 °C, and DAPI before observation via CLSM.

For flow cytometry (FC) analysis, BMDCs and splenocytes were respectively incubated with PASTA-NV or S17/TA-NV. After 4 h, the cells were washed and fixed with 1% PFA at 4 °C before FC measurements and analysis were performed via FlowJo v.10 software.

Biodistribution and Cellular Uptake Analysis of PASTA-NV In Vivo: All animal experiments were approved by the Animal Care and Use Committee of Soochow University, China (approval numbers: 202211A0251; 202212A0588; 202303A0754; 202309A0038), and all protocols for the animal studies conformed to the Guide for the Care and Use of Laboratory Animals. AML MLL-AF9 (MA9) mouse models were established via intravenous injection of 5×10^5 MA9 cells into C57BL/6 mice via the tail vein.

Cy5-labeled CpG was used as a probe for IVIS imaging of PASTA-NV after a single intravenous (i.v.) administration to MA9 mice. On day 3 postinoculation, PASTA-NV and S17/TA-NV were i.v. vaccinated via the tail vein (S17: 5 μg, CpG: 20 μg, Cy5: 0.18 μg per mouse). After 6 h, the spleen and inguinal lymph nodes (LNs) were collected for IVIS ex vivo imaging, FC staining, and immunofluorescence (IF) staining. For IF staining, frozen spleen and LN tissues (10 μm) were treated to distinguish B cells (CD45R (B220)), macrophages (F4/80), and DCs (CD11c) via CLSM.

To evaluate the impact of vaccination strategies on biodistribution, MA9 mice were vaccinated with three doses of PASTA-NV or S17/TA-NV, three i.v. injections (all i.v.), three s.c. injections (all s.c.), or a combination of two s.c. and one i.v. injection (s.c.+i.v.) on days 3, 6, and 9. For s.c. injection, nanovaccines were injected subcutaneously on both sides close to the inguinal LNs. The following treatment was the same as above.

Analysis of Immune Cell Infiltration and Activation In Vivo: AML mice were randomly divided and vaccinated with four doses of PASTA-NV or S17/TA-NV, via all i.v., all s.c., or s.c.+i.v. on days 3, 6, 9, and 16 (S17: 5 μg and CpG: 20 μg per mouse). On day 23, peripheral blood (PB) and tissue-derived single-cell suspensions (spleen, inguinal LNs, and bone marrow) were harvested via standardized processes and subject to an immunophenotyping protocol. These cells were collected and stained with Zombie-NIR, blocked with antimouse CD16/32, and subsequently stained with desired antibody cocktails (1:200 dilution) to identify subsets of DCs, NK cells, T cells, B cells, and macrophages. For staining of intracellular IFN-γ and TNF-α in CD8$^+$ T cells, the splenocytes were treated, permeabilized and stained with APC-conjugated anti-mouse IFN-γ and PerCP/Cy5.5-conjugated anti-mouse TNF-α (details in the supporting information). For $WT1_{126\text{-}134}$ tetramer staining, the splenocytes were stained with 50 μL of PE-labeled RMFPNAPYL-Tetramer plus FcR block at a 1:50 dilution for 30 min at room temperature in the dark, followed by a 20 min incubation with a premade 50 μL cocktail of surface antibodies (APC anti-mouse CD3 and FITC anti-mouse CD8a (clone: KT15) on ice in the dark.

All the stained cells described above were resuspended in RBC lysis/fixation solution for 10 min, washed and resuspended in PBS. The precision count beads were added, and the cells were transferred to 96-well plates (FALCON, 353 910) at 4 °C for FC measurement and analysis. The gating strategies are shown in Figure S9 (Supporting Information).

Analysis of Serum Samples: In the MA9 mice described above, PB samples were treated to detect a panel of inflammatory cytokines via a mouse inflammation panel according to the manufacturer's instructions. Serum levels of WT1-specific IgG and KRAS G12C-mutant epitope-specific IgG were measured via ELISA. Briefly, 96-well plates (Corning, Costar 9018) were coated overnight with the $WT1_{126\text{-}134}$ peptide (R9: RMFPNAPYL) or the KRAS G12C mutant peptide ($KRAS_{5\text{-}14}$: KLVVVGACGV) at a peptide concentration of 10 μg mL^{-1} at 4 °C. The plates were blocked with 1% BSA for 1 h at 37 °C and then incubated for 30 min with 100 μL of gradient dilutions of serum samples (100, 200, 400, 800, 1600, and 3200) at 37 °C. The following steps with HRP-conjugated IgG antibody and measurements were the same as those for a typical ELISA.

Antileukemia Efficacy in MA9 AML Models: On day 3 postinoculation, MA9 mice were randomly grouped and vaccinated with four doses of PASTA-NV or S17/TA-NV via all i.v., all s.c., or s.c.+i.v. at the same dose (S17: 5 μg and CpG: 20 μg per mouse) on days 3, 6, 9, and 16. The infiltration of MA9 cells in the PB and bone marrow was detected via FC according to the GFP signals. The body weight, health status, and survival of the mice were recorded. For combination therapy with anti-CTLA-4, MA9 mice were vaccinated with four doses of PASTA-NV via all i.v. or s.c.+i.v. as above and additionally i.v. injected with anti-CTLA-4 at 1 mg kg^{-1} on days 6, 9, and 16.

Long-Term Immune Memory Analysis: On day 60, blood samples from the surviving mice that received the above vaccines were withdrawn, blocked with anti-mouse CD16/32, and stained with APC-conjugated anti-mouse CD3, PE/Cy7-conjugated anti-mouse CD4, FITC-conjugated anti-mouse CD8, PerCP/Cy5.5-conjugated anti-mouse CD44 and PE-conjugated anti-mouse CD62L antibodies on ice. The cells were resuspended in RBC lysis/fixation solution for 10 min and washed before FC measurements of CD44$^+$CD62L$^+$ central memory T cells (T_{CM}) and CD44$^+$CD62L$^-$ effector memory T cells (T_{EM}).

On day 90, five surviving mice were rechallenged via i.v. injection of 5×10^5 MA9 cells. Naïve mice inoculated with MA9 cells were used as

controls. After 32 days, MA9 cells in the blood, body weight and survival of the mice were monitored as described above.

Ex-Vivo Specific Killing Generated by Vaccinated Mice: One surviving mouse that previously received PASTA-NV+Ab therapy was randomly selected. Splenocytes were isolated, counted and incubated overnight (5×10^6 mL^{-1}) with free R9 or S17 peptides in a 12-well plate at two peptide concentrations of 2.74 and 5.48 μM. The next day, these re-stimulated splenocytes were washed, counted and incubated with MA9 cells at a ratio of 10:1. After 24 h, all cells were collected and stained with Zombie-NIR. Living MA9 cells were detected by GFP signals (gated on all living cells) via FC.

Splenocytes restimulated with S17 peptides were added to MC38, GL261, or LLC cells seeded in 96-well plates at a ratio of 10:1. After 24 h of incubation, the cells were gently washed twice with PBS to remove splenocytes and dead cancer cells, and the viability of the tumor cells was determined via CCK-8 assays.

Statistical Analysis: Statistical analyses were performed via GraphPad Prism 8. The data were presented as the mean ± standard deviation (SD) unless stated otherwise. Mouse survival was analyzed via the log-rank (Kaplan–Meier) test. Significance of differences between two groups was determined via unpaired two-tailed Student's *t* tests. Significance in three or more groups was determined via one-way ANOVA and Tukey's multiple comparisons test. The *p* values are depicted as follows: * $p < 0.05$, ** $p < 0.01$, *** $p < 0.001$, and **** $p < 0.0001$.

Supporting Information

Supporting Information is available from the Wiley Online Library or from the author.

Acknowledgements

This work was supported by research grants from the National Key R&D Program of China (2022YFA1206000) and the National Natural Science Foundation of China (NSFC52033006, 52233007). The authors thank Biorender.com for assisting with the illustrations (https://BioRender.coms01f741).

Conflict of Interest

The authors declare no conflict of interest.

Data Availability Statement

The data that support the findings of this study are available from the corresponding author upon reasonable request.

Keywords

anticancer immune response, cancer vaccines, CpG, leukemia, peptide antigens, polymersomes

Received: August 31, 2024
Revised: November 13, 2024
Published online:

[1] a) C. H. June, R. S. O'Connor, O. U. Kawalekar, S. Ghassemi, M. C. Milone, *Science* **2018**, *359*, 1361; b) S. P. Kubli, T. Berger, D. V. Araujo, L. L. Siu, T. W. Mak, *Nat. Rev. Drug Discovery* **2021**, *20*, 899.

[2] P. J. Thul, L. Akesson, M. Wiking, D. Mahdessian, A. Geladaki, H. A. Blal, T. Alm, A. Asplund, L. Bjork, L. M. Breckels, A. Backstrom, F. Danielsson, L. Fagerberg, J. Fall, L. Gatto, C. Gnann, S. Hober, M. Hjelmare, F. Johansson, S. Lee, C. Lindskog, J. Mulder, C. M. Mulvey, P. Nilsson, P. Oksvold, J. Rockberg, R. Schutten, J. M. Schwenk, A. Sivertsson, E. Sjostedt, et al., *Science* **2017**, *356*, eaal3321.

[3] a) G. A. Roth, V. C. T. M. Picece, B. S. Ou, W. Luo, B. Pulendran, E. A. Appel, *Nat. Rev. Mater.* **2022**, *7*, 174; b) M. Yarchoan, E. J. Gane, T. U. Marron, R. Perales-Linares, J. Yan, N. Cooch, D. H. Shu, E. J. Fertig, L. T. Kagohara, G. Bartha, J. Northcott, J. Lyle, S. Rochestie, J. Peters, J. T. Connor, E. M. Jaffee, I. Csiki, D. B. Weiner, A. Perales-Puchalt, N. Y. Sardesai, *Nat. Med.* **2024**, *30*, 1044.

[4] a) M. S. Goldberg, *Nat. Rev. Cancer* **2019**, *19*, 587; b) P. J. Gawne, M. Ferreira, M. Papaluca, J. Grimm, P. Decuzzi, *Nat. Rev. Mater.* **2023**, *8*, 783.

[5] a) M. K. Fath, K. Babakhaniyan, M. Zokaei, A. Yaghoubian, S. Akbari, M. Khorsandi, A. Soofi, M. Nabi-Afjadi, H. Zalpoor, F. Jalalifar, A. Azargoonjahromi, Z. Payandeh, A. A. Bahrami, *Cell. Mol. Biol. Lett.* **2022**, *27*, 33; b) S. Shabani, S. Hadjigol, W. Li, Z. Si, D. Pranantyo, M. B. Chan-Park, N. M. O'Brien-Simpson, G. G. Qiao, *Nat. Rev. Bioeng.* **2024**, *2*, 343.

[6] a) R. Kuai, L. J. Ochyl, K. S. Bahjat, A. Schwendeman, J. J. Moon, *Nat. Mater.* **2017**, *16*, 489; b) S. L. Liu, Q. Jiang, X. Zhao, R. F. Zhao, Y. N. Wang, Y. M. Wang, J. B. Liu, Y. X. Shang, S. Zhao, T. T. Wu, Y. L. Zhang, G. J. Nie, B. Q. Ding, *Nat. Mater.* **2021**, *20*, 421; c) G. M. Lynn, C. Sedlik, F. Baharom, Y. L. Zhu, R. A. Ramirez-Valdez, V. L. Coble, K. Tobin, S. R. Nichols, Y. Itzkowitz, N. Zaidi, J. M. Gammon, N. J. Blobel, J. Denizeau, P. de la Rochere, B. J. Francica, B. Decker, M. Maciejewski, J. Cheung, H. Yamane, M. G. Smelkinson, J. R. Francica, R. Laga, J. D. Bernstock, L. W. Seymour, C. G. Drake, C. M. Jewell, O. Lantz, E. Piaggio, A. S. Ishizuka, R. A. Seder, *Nat. Biotechnol.* **2020**, *38*, 320.

[7] a) S. Pant, Z. A. Wainberg, C. D. Weekes, M. Furqan, P. M. Kasi, C. E. Devoe, A. D. Leal, V. Chung, O. Basturk, H. Vanwyk, A. M. Tavares, L. M. Seenappa, J. R. Perry, T. Kheoh, L. K. McNeil, E. Welkowsky, P. C. Demuth, C. M. Haqq, E. M. O'Reilly, *Nat. Med.* **2024**, *30*, 531; b) G. Middleton, P. Silcocks, T. Cox, J. Valle, J. Wadsley, D. Propper, F. Coxon, P. Ross, S. Madhusudan, T. Roques, D. Cunningham, S. Falk, N. Wadd, M. Harrison, P. Corrie, T. Iveson, A. Robinson, K. McAdam, M. Eatock, J. Evans, C. Archer, T. Hickish, A. Garcia-Alonso, M. Nicolson, W. Steward, A. Anthoney, W. Greenhalf, V. Shaw, E. Costello, D. Naisbitt, et al., *Lancet Oncol.* **2014**, *15*, 829; c) J. Schuster, R. K. Lai, L. D. Recht, D. A. Reardon, N. A. Paleologos, M. D. Groves, M. M. Mrugala, R. Jensen, J. M. Baehring, A. Sloan, G. E. Archer, D. D. Bigner, S. Cruickshank, J. A. Green, T. Keler, T. A. Davis, A. B. Heimberger, J. H. Sampson, *Neuro-Oncol* **2015**, *17*, 854; d) M. Weller, N. Butowski, D. D. Tran, L. D. Recht, M. Lim, H. Hirte, L. Ashby, L. Mechtler, S. A. Goldlust, F. Iwamoto, J. Drappatz, D. M. O'Rourke, M. Wong, M. G. Hamilton, G. Finocchiaro, J. Perry, W. Wick, J. Green, Y. He, C. D. Turner, M. J. Yellin, T. Keler, T. A. Davis, R. Stupp, J. H. Sampson, A. I. T. Investigators, *Lancet Oncol.* **2017**, *18*, 1373; e) M. S. Ahluwalia, D. A. Reardon, A. P. Abad, W. T. Curry, E. T. Wong, S. A. Figel, L. L. Mechtler, D. M. Peereboom, A. D. Hutson, H. G. Withers, S. Liu, A. N. Belal, J. Qiu, K. M. Mogensen, S. S. Dharma, A. Dhawan, M. T. Birkemeier, D. M. Casucci, M. J. Ciesielski, R. A. Fenstermaker, *J. Clin. Oncol.* **2023**, *41*, 1453; f) E. Massarelli, W. William, F. Johnson, M. Kies, R. Ferrarotto, M. Guo, L. Feng, J. J. Lee, T. Hai, Y. U. Kim, C. Haymaker, C. Bernatchez, M. Curran, T. Z. Barrese, J. R. Canales, I. Wistuba, L. Li, J. Wang, S. H. van der Burg, C. J. Melief, B. Glisson, *JAMA Oncol* **2019**, *5*, 67.

[8] a) G. Koehne, *Blood* **2017**, *130*, 1959. b) N. J. Shah, A. J. Najibi, T.-Y. Shih, A. S. Mao, A. Sharda, D. T. Scadden, D. J. Mooney, *Nat. Biomed. Eng.* **2020**, *4*, 40.

[9] M. A. Cheever, J. P. Allison, A. S. Ferris, O. J. Finn, B. M. Hastings, T. T. Hecht, I. Mellman, S. A. Prindiville, J. L. Viner, L. M. Weiner, L. M. Matrisian, *Clin. Cancer Res.* **2009**, *15*, 5323.
[10] a) T. Kiguchi, M. Yamaguchi, N. Takezako, S. Miyawaki, K. Masui, Y. Ihara, M. Hirota, N. Shimofurutani, T. Naoe, *Cancer Immunol. Immun.* **2022**, *71*, 1419; b) T. Naoe, A. Saito, N. Hosono, S. Kasahara, H. Muto, K. Hatano, M. Ogura, T. Masunari, M. Tanaka, K. Usuki, Y. Ishikawa, K. Ando, Y. Kondo, Y. Takagi, S. Takada, M. Ishikawa, I. Choi, A. Sano, H. Nagai, *Cancer Immunol. Immun.* **2023**, *72*, 2865.
[11] H. Khong, W. W. Overwijk, *J. ImmunoTher. Cancer* **2016**, *4*, 56.
[12] M. C. Sellars, C. J. Wu, E. F. Fritsch, *Cell* **2022**, *185*, 2770.
[13] B. Pulendran, P. S. Arunachalam, D. T. O'Hagan, *Nat. Rev. Drug Discovery* **2021**, *20*, 454.
[14] Y. Zhong, F. Meng, W. Zhang, B. Li, J. C. M. van Hest, Z. Zhong, *J. Controlled Release* **2020**, *320*, 421.
[15] a) Z. T. Hu, D. E. Leet, R. L. Allesoe, G. Oliveira, S. Q. Li, A. M. Luoma, J. Y. Liu, J. Forman, T. Huang, J. B. Iorgulescu, R. Holden, S. Sarkizova, S. H. Gohil, R. A. Redd, J. Sun, L. Elagina, A. Giobbie-Hurder, W. D. Zhang, L. Peter, Z. Ciantra, S. Rodig, O. Olive, K. Shetty, J. Pyrdol, M. Uduman, P. C. Lee, P. Bachireddy, E. I. Buchbinder, C. H. Yoon, D. Neuberg, et al., *Nat. Med.* **2021**, *27*, 515; b) H. Kobayashi, T. Nagato, N. Aoki, K. Sato, S. Kimura, M. Tateno, E. Celis, *Cancer Immunol. Immun.* **2006**, *55*, 850.
[16] Y. Zou, F. Meng, C. Deng, Z. Zhong, *J. Controlled Release* **2016**, *239*, 149.
[17] J. F. Brooks, J. Riggs, J. L. Mueller, R. Mathenge, W.-Y. Wholey, A. R. Meyer, S.-T. Yoda, V. S. Vykunta, H. V. Nielsen, W. Cheng, J. Zikherman, *Nat. Immunol.* **2023**, *24*, 1762.
[18] A. V. Krivtsov, D. Twomey, Z. Feng, M. C. Stubbs, Y. Wang, J. Faber, J. E. Levine, J. Wang, W. C. Hahn, D. G. Gilliland, T. R. Golub, S. A. Armstrong, *Nature* **2006**, *442*, 818.
[19] M. Guilliams, F. Ginhoux, C. Jakubzick, S. H. Naik, N. Onai, B. U. Schraml, E. Segura, R. Tussiwand, S. Yona, *Nat. Rev. Immunol.* **2014**, *14*, 571.
[20] L. Ma, T. Dichwalkar, J. Y. H. Chang, B. Cossette, D. Garafola, A. Q. Zhang, M. Fichter, C. Wang, S. Liang, M. Silva, S. Kumari, N. K. Mehta, W. Abraham, N. Thai, N. Li, K. D. Wittrup, D. J. Irvine, *Science* **2019**, *365*, 162.
[21] a) W. H. Fridman, M. Meylan, F. Petitprez, C.-M. Sun, A. Italiano, C. Sautes-Fridman, *Nat. Rev. Clin. Oncol.* **2022**, *19*, 441; b) L. Bod, Y.-C. Kye, J. Shi, E. T. Triglia, A. Schnell, J. Fessler, S. M. M. Ostrowski, M. Y. Y. Von-Franque, J. R. R. Kuchroo, R. M. M. Barilla, S. Zaghouani, E. Christian, T. M. Delorey, K. Mohib, S. Xiao, N. Slingerland, C. J. J. Giuliano, O. Ashenberg, Z. Li, D. M. M. Rothstein, D. E. E. Fisher, O. Rozenblatt-Rosen, A. H. H. Sharpe, F. J. J. Quintana, L. Apetoh, A. Regev, V. K. K. Kuchroo, *Nature* **2023**, *619*, 348.
[22] N. Veomett, T. Dao, H. Liu, J. Xiang, D. Pankov, L. Dubrovsky, J. A. Whitten, S.-M. Park, T. Korontsvit, V. Zakhaleva, E. Casey, M. Curcio, M. G. Kharas, R. J. O'Reilly, C. Liu, D. A. Scheinberg, *Clin. Cancer Res.* **2014**, *20*, 4036.
[23] C. Cui, J. Wang, E. Fagerberg, P.-M. Chen, K. A. Connolly, M. Damo, J. F. Cheung, T. Mao, A. S. Askari, S. Chen, B. Fitzgerald, G. G. Foster, S. C. Eisenbarth, H. Zhao, J. Craft, N. S. Joshi, *Cell* **2021**, *184*, 6101.
[24] A. S. Bear, T. Blanchard, J. Cesare, M. J. Ford, L. P. Richman, C. Xu, M. L. Baroja, S. McCuaig, C. Costeas, K. Gabunia, J. Scholler, A. D. Posey, M. H. O'Hara, A. Smole, D. J. Powell, B. A. Garcia, R. H. Vonderheide, G. P. Linette, B. M. Carreno, *Nat. Commun.* **2021**, *12*, 4365.
[25] L. Ma, A. Hostetler, D. M. Morgan, L. Maiorino, I. Sulkaj, C. A. Whittaker, A. Neeser, I. S. Pires, P. Yousefpour, J. Gregory, K. Qureshi, J. Dye, W. Abraham, H. Suh, N. Li, J. C. Love, D. J. Irvine, *Cell* **2023**, *186*, 3148.
[26] a) S. Ols, L. F. Yang, E. A. Thompson, P. Pushparaj, K. Tran, F. Liang, A. Lin, B. Eriksson, G. B. K. Hedestam, R. T. Wyatt, K. Loré, *Cell Rep.* **2020**, *30*, 3964; b) F. Baharom, R. A. Ramirez-Valdez, K. K. S. Tobin, H. Yamane, C. A. Dutertre, A. Khalilnezhad, G. Reynoso, V. L. Coble, G. M. Lynn, M. P. Mule, A. J. Martins, J. P. Finnigan, X. M. Zhang, J. A. Hamerman, N. Bhardwaj, J. S. Tsang, H. D. Hickman, F. Ginhoux, A. S. Ishizuka, R. A. Seder, *Nat. Immunol.* **2021**, *22*, 41.
[27] a) Y. O. Alexandre, S. N. Mueller, *Nat. Rev. Immunol.* **2023**, *23*, 705; b) D. Liu, B. Y. Winer, M. Y. Chou, H. Tam, Y. Xu, J. An, J. M. Gardner, J. G. Cyster, *Nat. Immunol.* **2024**, *25*, 142.
[28] T. Karakousi, T. Mudianto, A. W. Lund, *Nat. Rev. Cancer* **2024**, *24*, 363.
[29] J. Svensson-Arvelund, S. Cuadrado-Castano, G. Pantsulaia, K. Kim, M. Aleynick, L. Hammerich, R. Upadhyay, M. Yellin, H. Marsh, D. Oreper, S. Jhunjhunwala, C. Moussion, M. Merad, B. D. Brown, A. Garcia-Sastre, J. D. Brody, *Nat. Commun.* **2022**, *13*, 7149.
[30] a) F. Baharom, R. A. Ramirez-Valdez, A. Khalilnezhad, S. Khalilnezhad, M. Dillon, D. Hermans, S. Fussell, K. K. S. Tobin, C.-A. Dutertre, G. M. Lynn, S. Muller, F. Ginhoux, A. S. Ishizuka, R. A. Seder, *Cell* **2022**, *185*, 4317; b) L. Cassetta, J. W. Pollard, *Nat. Rev. Cancer* **2023**, *23*, 238.
[31] a) F. S. Hodi, S. J. O'Day, D. F. McDermott, R. W. Weber, J. A. Sosman, J. B. Haanen, R. Gonzalez, C. Robert, D. Schadendorf, J. C. Hassel, W. Akerley, A. J. M. van den Eertwegh, J. Lutzky, P. Lorigan, J. M. Vaubel, G. P. Linette, D. Hogg, C. H. Ottensmeier, C. Lebbe, I. Peschel, J. I. Quirt, J. D. Clark, J. S. Wolchok, J. Weber, M. J. Tian, G. M. Yellin, A. Nichol, W. J. Hoos, *N. Engl. J. Med.* **2010**, *363*, 711; b) S. C. Formenti, N.-P. Rudqvist, E. Golden, B. Cooper, E. Wennerberg, C. Lhuillier, C. Vanpouille-Box, K. Friedman, L. F. de Andrade, K. W. Wucherpfennig, A. Heguy, N. Imai, S. Gnjatic, R. O. Emerson, X. K. Zhou, T. Zhang, A. Chachoua, S. Demaria, *Nat. Med.* **2018**, *24*, 1845.
[32] P. Zhang, T. Wang, G. Cui, R. Ye, W. Wan, T. Liu, Y. Zheng, Z. Zhong, *Adv. Mater.* **2024**, *36*, 2407189.
[33] L. K. Mackay, A. Braun, B. L. Macleod, N. Collins, C. Tebartz, S. Bedoui, F. R. Carbone, T. Gebhardt, *J. Immunol.* **2015**, *194*, 2059.
[34] P. Kvistborg, D. Philips, S. Kelderman, L. Hageman, C. Ottensmeier, D. Joseph-Pietras, M. J. P. Welters, S. van der Burg, E. Kapiteijn, O. Michielin, E. Romano, C. Linnemann, D. Speiser, C. Blank, J. B. Haanen, T. N. Schumacher, *Sci. Transl. Med.* **2014**, *6*, 254ra128.
[35] a) X. He, S. Zhou, B. Quinn, D. Jahagirdar, J. Ortega, M. D. Long, S. I. Abrams, J. F. Lovell, *Cancer Immunol. Res.* **2022**, *10*, 314; b) S. Zhou, Y. Song, Y. Luo, B. Quinn, Y. Jiao, M. D. Long, S. I. Abrams, J. F. Lovell, *Cancer Res. Commun.* **2024**, *4*, 958.